Physics informed neural networks for Triple Deck

Journal:	*Aircraft Engineering and Aerospace Technology*
Manuscript ID	AEAT-10-2021-0309.R2
Manuscript Type:	Research Paper
Keywords:	PINN's, Triple Deck, Asymptotic, Flow control

Physics informed neural networks for Triple Deck

Purpose – This paper introduces physics-informed neural networks (PINN) applied to the two-dimensional steady-state laminar Navier-Stokes equations over a flat plate with roughness elements and specified local heating. The method bridges the gap between asymptotics theory and three-dimensional turbulent flow analyses, characterised by high costs in analysis setups and prohibitive computing times. The results indicate the possibility of using surface heating or wavy surface to control the incoming flow field.

Design/methodology/approach – The understanding of the flow control mechanism is normally caused by the unsteady interactions between the aircraft structure and the turbulent flows as well as some studies have shown, surface roughness can significantly influence the fluid dynamics by inducing perturbations in the velocity profile.

Findings – The description of the boundary-layer flow, based upon a Triple-Deck structure, shows how a wavy surface and a local surface heating generate an interaction between the inviscid region and the viscous region near the flat plate.

Originality/value–The presented approach is especially original in relation to the innovative concept of physics-informed neural networks as a solver of the asymptotic triple deck method apply to the viscous-inviscid boundary layer interaction.

Keywords PINN's, Triple Deck, Asymptotic, Flow control.

Paper type: Research paper.

1 Introduction

Triple-Deck Theory (TdT) developed by Lighthill (Lighthill, 1952), is a theory that describes a three-layered boundary-layer structure when disturbances are present in the boundary layer. The theoretical approach takes into account the influence of viscosity on a disturbance to an incident boundary-layer profile. The physical process is referred to as a pressure–displacement (or viscous–inviscid) interaction. The inviscid flow outside the boundary layer, the displaced boundary layer in

which the perturbations are governed by linearized compressible Euler equations, and an inner part close to the wall in which the perturbations are governed by incompressible boundary-layer equations.

Independently Neiland (Neiland, 1969), Stewartson (Stewartson, 1969), Stewartson and Williams (Williams et al., 1969), and Messiter (Messiter, 1970) extended Lighthill's theory to non-linear interactions. They used Gadd's approximation to modify the TdT to overcome the singularities in the boundary-layer solutions at the separation point and the edge of the flat plate (Gadd, 1957).

Hunt (Hunt, 1971) and Smith (Smith, 1973), using order of magnitude arguments, investigated the structure of an incompressible flow at a high Reynolds number past a hump on an otherwise smooth surface. In these cases, the TdT is able to accurately describe the interaction between the boundary layer flow and inviscid flow outside the boundary layer.

The TdT was extended to include unsteady flows by Schneider (Schneider, 1974). It was noted that the flow in the viscous lower deck was the most sensitive to unsteady perturbations. The asymptotic foundation of two-dimensional, steady-state TdT (for incompressible and compressible flows) was reviewed by Zeytounian (Zeytounian, 2003). Diesperov and Korolev (Diesperov et al., 2003) investigated the transonic flow past a small hump on a flat plate by solving the Triple-deck equations.

Recently, Lipatov and Koroteev have published a series of papers (see for instance Lipatov (Lipatov, 2006), Koroteev and Lipatov (2008, 2009, 2012, 2013)) in which micro-electro-mechanical-system (MEMS) devices are modelled as small flat-plate localised heating elements located in the boundary layer. The work of Mengaldo (Mengaldo et al., 2015) who looked at subsonic and transonic flows over roughness elements, suggests that TdT is able to correctly capture the main qualitative physics in practical aeronautical applications.

This paper investigates the possibility of using the non-linear lower deck approach of the TdT of the viscous-inviscid interactions due to a wavy surface and a local heating surface. More precisely, the aim is to gain a better understanding, from a mathematical perspective, of how surface waviness can be used to change the flow properties. For instance, it is shown in the case of the aircraft, if we

consider large typical Reynolds numbers and assume the characteristic size of a wing-fuselage to be 4 m, then the size of the interaction region in the TdT is approximately 1 cm. These methods could be applied for flow control on wings. An outline of the paper is as follows: In the next section, we detail the triple-deck model, the appropriately scaled governing equations and boundary conditions. Additionally, the physics-informed neural networks method for solving lower-deck equations is introduced. In Section 3, the results of the non-linear calculations are examined for increasing heights of rippled surfaces and different local temperature amplitudes. Finally, some conclusions are drawn in Section 4.

2 TRIPLE-DECK ANALYSIS

A laminar, incompressible, two-dimensional, steady flow over a flat plate is considered. Two cases are studied: a wavy surface and a local surface heating. The incoming flow is uniform and, therefore, irrotational. We assume that the perturbation produced by the boundary layer on the inviscid flow is of order ε (Eqn. 1) for the velocity components and the pressure.

$$\varepsilon = \frac{1}{R_e{}^m}, \quad where \quad m \quad is \quad arbitrary \quad (m > 0) \tag{1}$$

The two dimensionless Navier-Stokes equations in terms of dimensionless variables are given by:

$$\frac{\partial u}{\partial x} + \frac{\partial v}{\partial y} = 0$$

$$u\frac{\partial u}{\partial x} + v\frac{\partial u}{\partial y} = -\frac{\partial p}{\partial x} + \frac{1}{R_e}\frac{\partial^2 u}{\partial x^2} + \frac{1}{R_e}\frac{\partial^2 u}{\partial y^2} \tag{2}$$

$$u\frac{\partial v}{\partial x} + v\frac{\partial v}{\partial y} = -\frac{\partial p}{\partial y} + \frac{1}{R_e}\frac{\partial^2 v}{\partial x^2} + \frac{1}{R_e}\frac{\partial^2 v}{\partial y^2}$$

The scaling of this problem requires a division of the vertical structure into a Triple-Deck regime as shown in Figure 1: a viscous sublayer (’Lower Deck’) and an inviscid main part of the boundary layer (’Main Deck’), where the third tier is an inviscid potential flow (’Upper Deck’) outside of the boundary layer. The Triple-Deck structure establishes a link between the unperturbed upstream flow and the downstream flow.

Figure 1: Triple deck structure (Mauss et al., 2007)

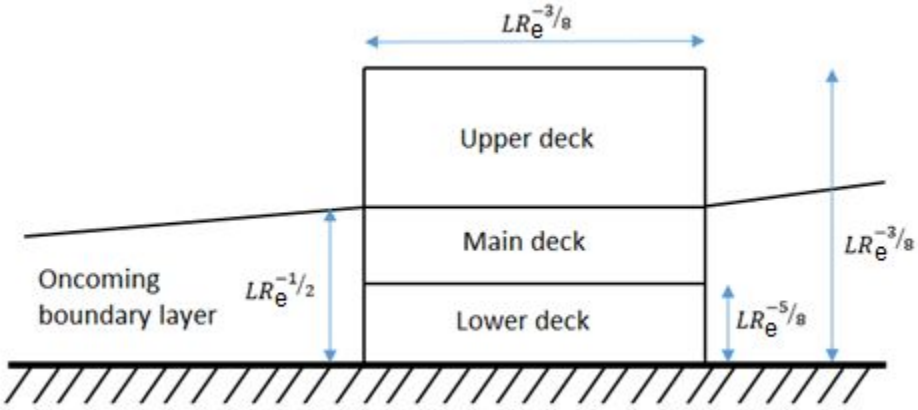

The longitudinal and transverse length scales of the perturbed region are $LR_e^{\frac{-3}{8}}$. Inside the perturbed region, there are three decks.

• First, the "Lower Deck": the thickness of the lower deck is $LR_e^{\frac{-5}{8}}$, is comprised of the stream filaments immediately adjacent to the wall. Even a small variation of pressure along the wall may cause significant deceleration/acceleration of fluid particles. As a result, the flow filaments change their thickness leading to a deformation of streamlines. This process is termed the displacement effect of the boundary layer. The perturbations in this lower layer are transmitted through the "Main Deck".

• The basic boundary layer is now the "Main Deck". The flow in this tier is significantly less sensitive to pressure variations. It does not produce any noticeable contribution to the displacement effect of the boundary layer.

• Finally, the upper tier. It serves to convert the perturbations in the form of the streamlines into perturbations of pressure. These are then transmitted through the main part of the boundary layer back to the "Lower Deck", enhancing the process of fluid deceleration.

As in all Triple-Deck problems, it reduces to solving the lower-deck equations. These, in turn, will provide solutions for the main and upper decks.

The structure of the Triple Deck is:

$$Y^* = \frac{y}{\varepsilon^{\alpha}} \quad \overline{Y} = Y = \frac{y}{\varepsilon^{m/2}} \quad \tilde{Y} = \frac{y}{\varepsilon^{(4\alpha+m)/4}}$$

Upper deck

- $u = 1 + \varepsilon^{m-2\alpha} U_1^* + \ldots,$
- $v = \varepsilon^{m-2\alpha} V_1^* + \ldots,$
- $p = \varepsilon^{m\alpha-2\alpha} P_1^* + \ldots,$

- $\frac{\partial U_1^*}{\partial X} + \frac{\partial V_1^*}{\partial Y^*} = 0,$
- $\frac{\partial U_1^*}{\partial X} = -\frac{\partial P_1^*}{\partial X},$
- $\frac{\partial V_1^*}{\partial X} + \frac{d^2 f}{dX^2} = -\frac{\partial P_1^*}{\partial Y^*}.$

(3)

Main deck

- $u = U_0 + \varepsilon^{(m-2\alpha)/2} \overline{U}_1 + \ldots,$
- $v = \varepsilon^{m-2\alpha} \overline{V}_1 + \ldots,$
- $p = \varepsilon^{m-2\alpha} \overline{P}_1,$

- $\frac{\partial \overline{U}_1}{\partial X} + \frac{\partial \overline{V}_1}{\partial \overline{Y}} = 0,$
- $U_0 \frac{\partial \overline{U}_1}{\partial X} + \overline{V}_1 \frac{dU_0}{d\overline{Y}} = 0,$
- $\frac{\partial \overline{P}_1}{\partial \overline{Y}} = 0.$

(4)

Lower deck

- $u = \varepsilon^{(m-2\alpha)/2} \tilde{U}_1 + \varepsilon^{(3\alpha-\beta)/4} \lambda \tilde{Y} + \ldots,$
- $v = \varepsilon^{(3m-4\alpha)/4} \tilde{V}_1 + \ldots,$
- $p = \varepsilon^{m-2\alpha} \tilde{P}_1 + \ldots,$

- $\frac{\partial \tilde{U}_1}{\partial X} + \frac{\partial \tilde{V}_1}{\partial \tilde{Y}} = 0,$
- $\tilde{U}_1 \frac{\partial \tilde{U}_1}{\partial X} + \tilde{V}_1 \frac{\partial \tilde{U}_1}{\partial \tilde{Y}} = -\frac{\partial \tilde{P}_1}{\partial X} + \frac{\partial^2 \tilde{U}_1}{\partial \tilde{Y}^2}$
- $\frac{\partial \tilde{P}_1}{\partial \tilde{Y}} = 0.$

(5)

2.1 MAIN DECK

The Eqns. 4 are solved.give:

$$-U_0 \frac{\partial \overline{V}_1}{\partial Y} + \overline{V}_1 \frac{dU_0}{d\overline{Y}} = 0 \tag{6}$$

Dividing both terms by U_0^2, the Eqn. 6 become $-\frac{1}{U_0}\frac{\partial \overline{V}_1}{\partial Y} + \overline{V}_1 \frac{U_0'}{U_0^2} = 0$ or equivalently $\frac{\partial}{\partial Y}\left(\frac{\overline{V}_1}{U_0}\right) = 0$

The ratio $\frac{\overline{V}_1}{U_0}$ is a function of X only, $\overline{V}_1$ become $-\frac{dA}{dX} U_0$ where $A(X)$ is an unknown displacement function.

In the main deck, the solution is given by:

$$\overline{U}_1 = A(X)U_0'(\overline{Y}) \quad with \quad U_0'(\overline{Y}) = \frac{dU_0}{d\overline{Y}}$$

$$\overline{V}_1 = -A'(X)U_0(\overline{Y}) \quad with \quad A'(X) = \frac{dA}{dX} \tag{7}$$

$$P_1 = \overline{P}_1(X)$$

The appropriate form of the solution to the resulting equations is:

$$u = U_0 + \varepsilon^{(m-2\alpha)/2}A(X)U_0'(\overline{Y}) + ...,$$

$$v = -\varepsilon^{m-2\alpha}A'(X)U_0(\overline{Y}) + ..., \tag{8}$$

$$p = \varepsilon^{m-2\alpha}\overline{P}_1.$$

$A(X)$ can be interpreted as the velocity slip at the base of the main deck corresponding to the inviscid perturbation of the upstream Blasius solution by the induced pressure gradient.

2.2 LOWER DECK

The initial conditions are given by:

- $X \to -\infty$ is satisfied provided $A(-\infty) = 0$.
- On the surface waviness $Y = f(X)$ no-slip conditions $\tilde{U}_1 = 0$, $\tilde{V}_1 = 0$, $\frac{\partial \tilde{U}_1}{\partial \tilde{Y}} = 0$
- $\lim_{\tilde{Y}\to\infty}(\tilde{U}_1 - \lambda\tilde{Y}) = \lambda(A + f)$, or $\tilde{U}_1 \to \lambda(\tilde{Y} + A + f)$, as $\tilde{Y} \to \infty$.

The conditions which relate the displacement thickness with the longitudinal velocity are supplied with the interaction condition, which in turn, relates the displacement thickness with the pressure and thus expresses the interaction of the viscous sublayer with the outer inviscid flow (Lipatov et al. 2011).

2.3 UPPER DECK

The first term in the upper deck is 1. The value of the first approximation for the inviscid flow outside the boundary layer from matching the solutions between the upper layer (as $Y^* \to 0$) and main layer (as $\overline{Y} \to \infty$) is:

$$
\begin{aligned}
&a)\quad Y^{*}\to 0:\quad U_0\to 1\quad U_1^{*}=0;\\
&b)\quad V_1^{*}=-\frac{\partial f}{\partial X};\\
&c)\quad V_1^{*}(X,0)=\lim_{\overline{Y}\to\infty}\overline{V}_1(X,\overline{Y});\\
&d)\quad V_1^{*}(X,0)=-\frac{dA}{dX};\\
&e)\quad P_1^{*}(X,0)=-U_1^{*}(X,0);\\
&f)\quad P_1^{*}(X,0)=\lim_{\tilde{Y}\to\infty}\tilde{P}_1(X,\tilde{Y}).
\end{aligned}
\tag{9}
$$

Moreover, as we have $\frac{\partial \overline{P}_1}{\partial \overline{Y}}=0$ and $\frac{\partial \tilde{P}_1}{\partial \tilde{Y}}=0$, we deduce that: $P_1^{*}(X,0)=\overline{P}_1(X)=\tilde{P}_1(X)$.

The Triple-Deck displacement function, $A(X)$, is related to the air pressure through the Cauchy-Hilbert integral:

$$\tilde{P}_1(X)=\frac{1}{\pi}\int_{-\infty}^{\infty}\frac{\frac{\partial}{\partial\xi}(A-f)}{X-\xi}d\xi \tag{10}$$

2.4 NUMERICAL SOLUTION OF TRIPLE DECK

To find the resulting flow field and in particular the displacement function and pressure it is necessary to solve the non-linear lower-deck equation. Apart from the non-linearity of the governing equations, complications arise from the elliptic nature of the Hilbert integral pressure displacement relationship. One relationship between the unknown pressure P and displacement A is obtained from the potential flow properties holding in the upper deck outside the boundary layer (Smith 1973; Stewartson 1974).

The Lower Deck equations taking into account the asymptotic scales and the Hilbert integral are:

- Flow past a shape:

$$\frac{\partial \tilde{U}_1}{\partial X}+\frac{\partial \tilde{V}_1}{\partial \tilde{Y}}=0 \tag{11}$$

$$\tilde{U}_1\frac{\partial \tilde{U}_1}{\partial X}+\tilde{V}_1\frac{\partial \tilde{U}_1}{\partial \tilde{Y}}=-\frac{\partial \tilde{P}_1}{\partial X}+\frac{\partial^2 \tilde{U}_1}{\partial \tilde{Y}^2}$$

$$\frac{\partial \tilde{P}_1}{\partial \tilde{Y}}=0$$

$$\frac{\partial \tilde{P}_1}{\partial X}(X)=-\frac{1}{\pi}\int_{-\infty}^{\infty}\frac{A''(\xi)-f''(\xi)}{\xi-X}d\xi \quad (12)$$

• In order to obtain wall heat and transfer for interacting flows, the asymptotic form of the energy equation resulting from a triple-deck analysis must be solved (Lipatov, 2006) (Lipatov et al., 2011), (Lipatov et al., 2012) :

$$\begin{aligned}&\frac{\partial \tilde{U}_1}{\partial X}+\frac{\partial \tilde{V}_1}{\partial \tilde{Y}}=0\\&\tilde{U}_1\frac{\partial \tilde{U}_1}{\partial X}+\tilde{V}_1\frac{\partial \tilde{U}_1}{\partial \tilde{Y}}+T\frac{\partial \tilde{P}_1}{\partial X}=\frac{\partial^2 \tilde{U}_1}{\partial \tilde{Y}^2}\\&\tilde{U}_1\frac{\partial \tilde{T}_1}{\partial X}+\tilde{V}_1\frac{\partial \tilde{T}_1}{\partial \tilde{Y}}+=\frac{\partial^2 \tilde{T}_1}{\partial \tilde{Y}^2}\end{aligned} \quad (13)$$

$$\frac{\partial \tilde{P}_1}{\partial X}(X)=-\frac{1}{\pi}\int_{-\infty}^{\infty}\frac{A''(\xi)}{\xi-X}d\xi \quad (14)$$

The basic problem was solved by using PINN's approach introduced recently by Raissi (Raissi et al. 2017 and 2019). We can replace traditional numerical discretization methods with a neural network that approximates the solution to a PDE. To obtain the approximate solution of a PDE via deep learning, a key step is to constrain the neural network to minimize the PDE residual. Compared to traditional mesh-based methods, such as the finite difference method (FDM) and the finite element method (FEM), deep learning could be a mesh-free approach by taking advantage of automatic differentiation. The optimizer is used after the comparison between target values and outputs of the network and the goal is to minimize the loss function by adjusting model parameters (weights and biases). There are different types of optimisers. Each type of optimiser has its own merits. The most common optimizers are Adam and the L-BFGS-B (Limited-memory Broyden-Fletcher-Goldfarb-Shanno Bound) (DU, Ke-Lin et al., 2014). When training the network, we prefer starting with Adam optimizer rather than L-BFGS-B, because this latter has more probability to get stuck on a local minimum.

The PINN introduces physical information into the network by forcing the network output to satisfy the corresponding partial differential equations. Neural networks (NN) are a set of algorithms, inspired by the biological neural networks in brains, for classification and regression tasks. A NN defines a mapping from the input layer $z_0 \in \mathbb{R}^{n_0}$ to the output $z_L \in \mathbb{R}^{n_L}$. The layers between the input and output layers are called hidden layers z_l, where $l = 1,...,L-1$. By convention, a neural network with more than one hidden layer is called a "deep" NN. Mathematically, two adjacent layers are connected as,

$$z_l = \sigma_l(w_l^T z_{l-1} + b_l)$$

Between each layer, a weight matrix "$w_l \in \mathbb{R}^{n_{l-1} \times n_l}$" and bias vector "$b_l \in \mathbb{R}^{n_l}$" are applied, the subscript l denotes the index of the layer; $\sigma_l(\cdot)$ is an activation function. Feed-forward neural networks are composed of the input layer, fully connected hidden layers having a nonlinear activation function at each neuron, and the output layer. Figure 2 (a and b) shows a general architecture of PINN and details its application to solve the Triple-Deck system. The PINN's framework consists of two parts. The first part is a neural network NN(w, b) that takes the coordinate (x,y) as the input and outputs predict five scalar state variables, i.e., velocity (u,v), pressure p, temperature T, and displacement of the fluid flow. The NN architecture is composed of eight (8) hidden layers, with one hundred (100) neurons per layer, and a hyperbolic tangent tanh is chosen as the Swish activation function.

Then, the output of NN is fed into a second part, which is essentially the governing differential equations of the lower deck and the Hilbert integral, to evaluate the pressure gradient of the Triple-Deck equations. The physics loss function is the summation of the governing loss, the initial and boundary condition loss given by:

$$MSE_u = MSE_{i/bc} + MSE_f \quad (15)$$

The calculation of the mean square error (MSE) is given by the following formula:

$$MSE_{i/bc} = \frac{1}{N_{i/bc}} \sum_{j=1}^{N_{i/bc}} |u^i - u|^2 \quad (16)$$

$$MSE_f = \frac{1}{N_g} \sum_{j=1}^{N_g} |f|^2 \quad (17)$$

During training, weight matrices and biases are optimized to find the best neural network parameters that minimize the loss function

$$\{w^*, b^*\} = arg \min_{\{w,b\}} \{MSE_u(w,b)\}$$

For the optimization procedure, we set the learning rate to 0.001, and in order to balance convergence speed and global convergence, we ran L-BFGS-B 500,000 epochs and then continued the optimization using Adam until convergence.

Figure 2: The schematic of PINN for solving TdT with Smith (Smith et al, 1981) method

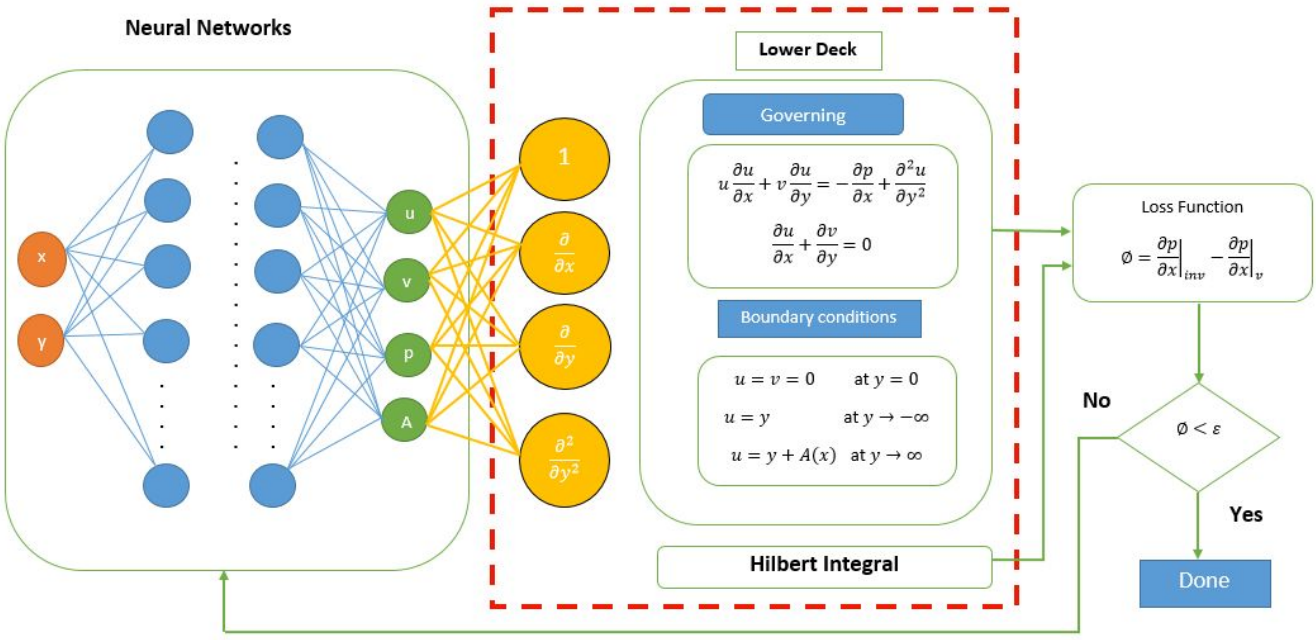

(a)

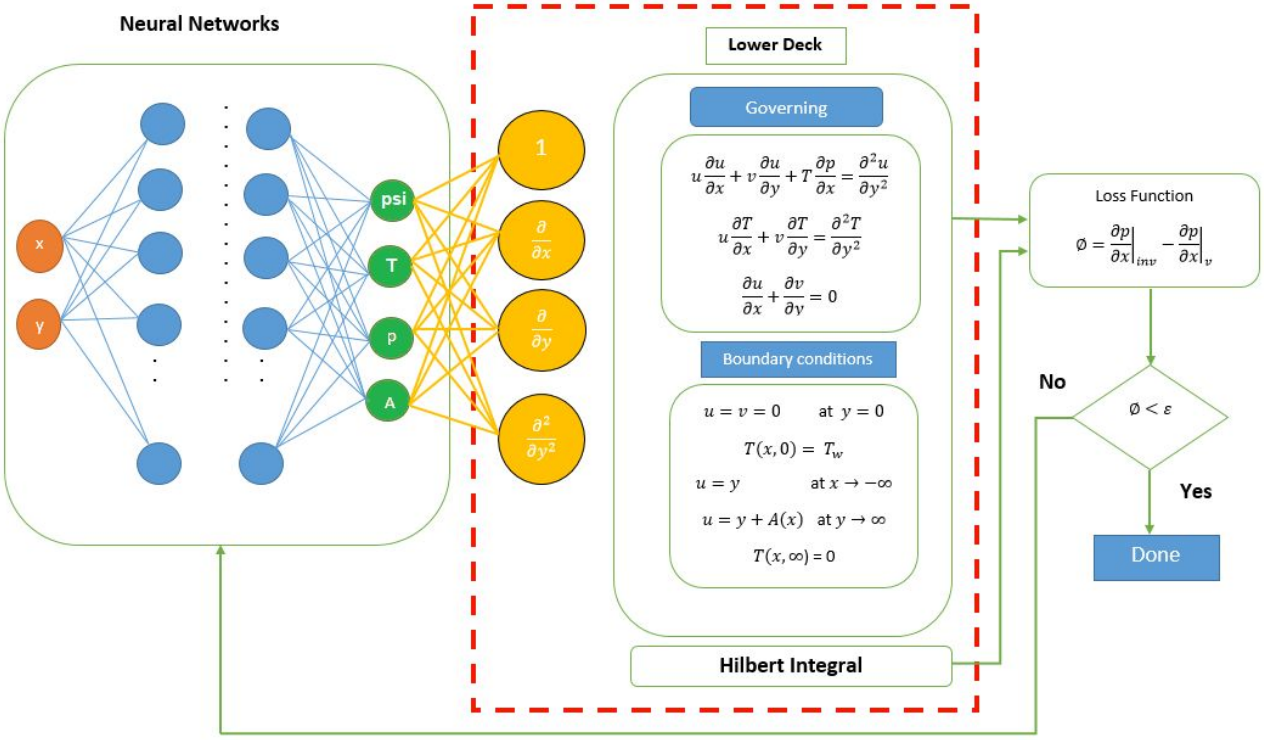

(b)

Eqn. (16) requires the neural network to satisfy the initial and boundary conditions, while Eqn. (17) requires the neural network to satisfy the constraints of the partial differential equation, which corresponds to the physical information part of the neural network. Given the displacement "A", Eqn. (10) allows calculation of the "inviscid pressure gradient", $\frac{\partial P}{\partial X}|_{inv}$. On the other hand, we calculate the "viscous pressure gradient", $\frac{\partial P}{\partial X}|_{v}$, based on the Eqns. (11) or (13). The optimization problem for Eqn. (15) is addressed by optimizing the parameters in order to find the minimum value of the loss function.

To validate the prediction performance of the trained PINN, corresponding CFD simulations are also conducted using an open CFD solver, OpenFOAM version 2.4.0 stands for (Open Source Field Operation And Manipulation), (https://openfoam.org). We will be using PISO (Pressure Implicit with Splitting of Operator) algorithm implemented in pisoFoam solver. The time discretization is performed by the implicit Crank-Nicolson scheme with a coefficient of 0.5. The Gaussian-type schemes are chosen for the spatial (gradient, divergence, and laplacian) discretization. The Poisson equation for pressure is solved by GAMG (Generalized Geometric-Algebraic Multi-Grid) algorithm,

while the linear equation for velocity is solved by PBiCG algorithm (Preconditioned Bi-Conjugate gradient solver for asymmetric matrices). Linear interpolation is used to obtain the physical quantities at the surface centers of the cells.

3 Results and discussion

In this section, we present results from the numerical solution of the non-linear Triple-Deck problem for subsonic flow past different geometries (humps or Gaussian shape, hump-dip Figure 3) and a heated part on the surface of the plate (Figure 10), respectively, located at a distance L_0 from the leading edge. We discuss the numerical data for the two functions, $A(X)$ and $P(X)'$, with the predicted asymptotic method (TdT) coupling with the PINN's techniques. Satisfying the asymptotic boundary conditions is of major importance in assessing the accuracy of the numerical procedure.

3.1 FLAT PLATE WITH SHAPED FORMS

New results have been presented, obtained by PINN technics, which serve to identify the effects of roughness elements as represented in Figure 3 in the distribution of the displacement and pressure. They also constitute a concrete step towards understanding the mechanism of momentum transfer between inviscid flow outside and viscous sub-layer. The shape of the roughness element was given by:

- Hump shape equation: $f(x) = h_r exp(-(L_r - x)^2/\beta^2)$
- Ripped shape equation: $f(x) = h_r sin(\frac{2\pi}{L}x)$

where L_r is the distance from the center of the roughness element to the leading edge of the flat plate, h_r is the height of the roughness element and β is a parameter that controls the shape of the roughness element. In particular, L_0 and β were fixed and equal to $0.05m$ and $1.7961 * 10^{-4}m$, respectively. Concerning the height of the roughness element, we took into account four different values: $h_r = [0, \frac{1}{8}, \frac{2}{8}, \frac{4}{8}]Y_{Lower}$, where $Y_{Lower} = L_0 R^{\frac{-3}{8}}$ is the thickness of the lower deck.

Figure 3: flat plate deformed by rippled shapes

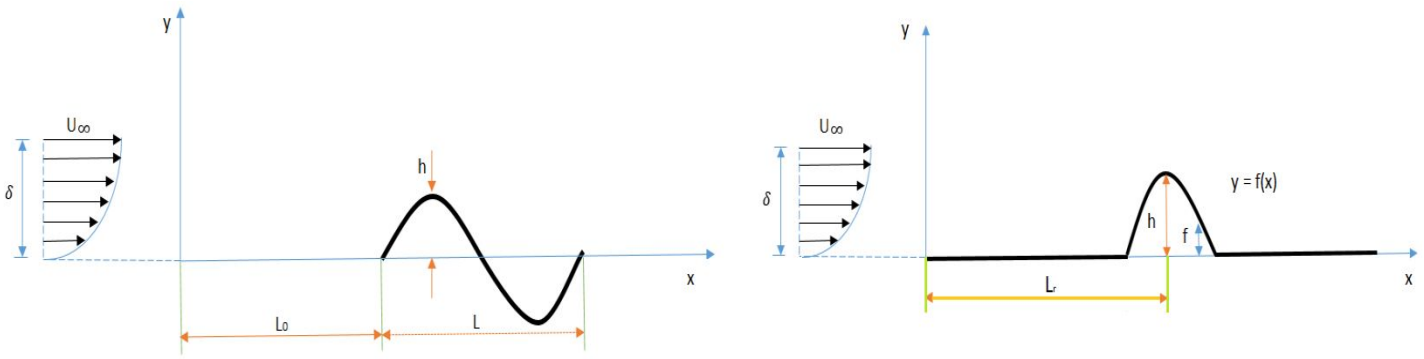

The results of the calculations are summarized in Figures 4, 5, 6 and 7, which shows the comparison of the velocity upper the rippled surface, the displacement function $A(x)$, the displacement gradient $\frac{dA}{dx}$ and the pressure gradient $\frac{dp}{dx}$ as a function of the scaled length.

Figure 4: Comparison of the four predictions for hump case

(a) Axial velocity; (b) pressure gradient, (c) Displacement; (d) displacement gradient

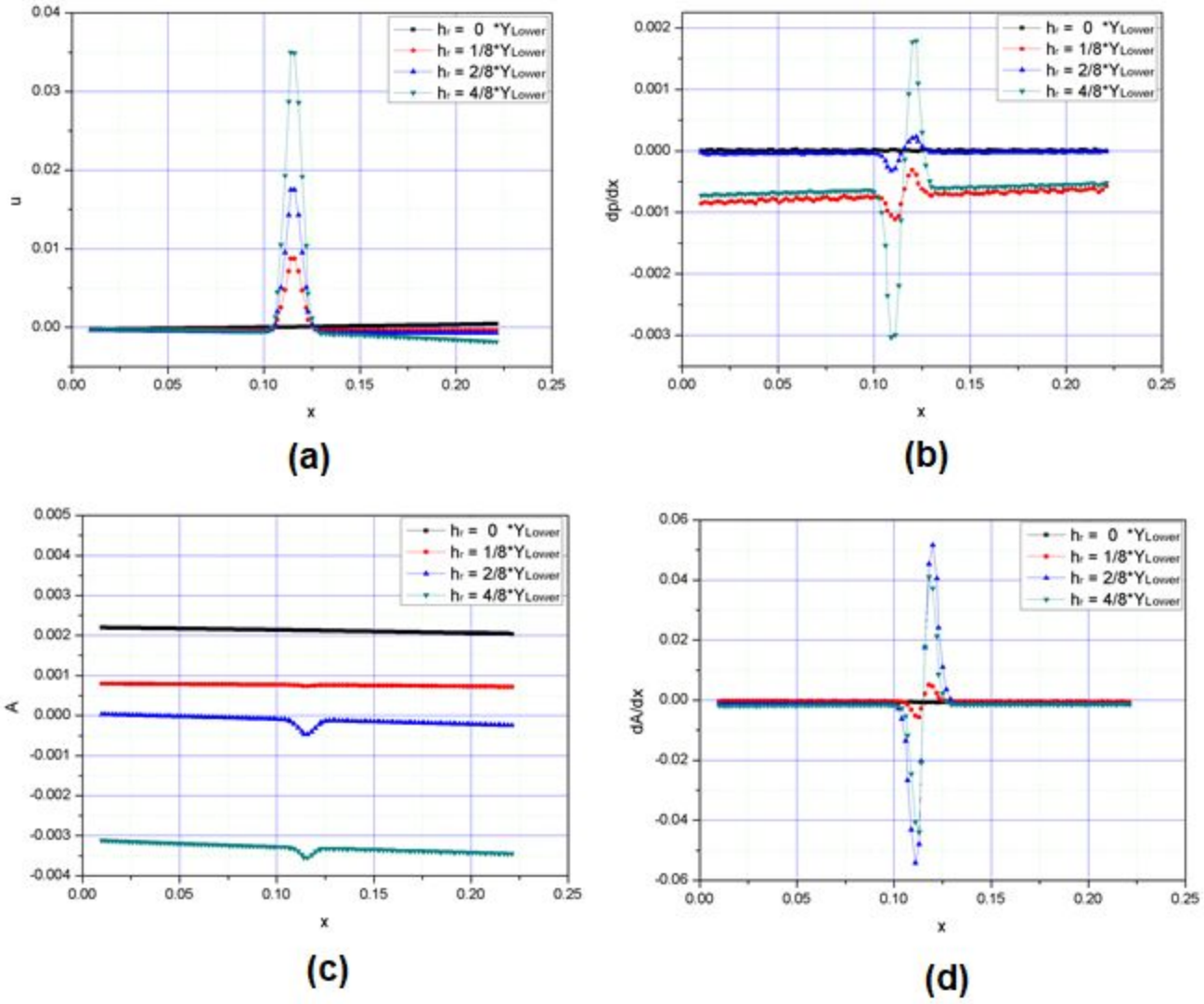

The detailed results of the Triple-Deck analysis show that the predominant effect of the rippled surface on the boundary layer is to cause a local distortion in the pressure. We have seen that far upstream, where the interaction region matches with the unperturbed boundary layer, the displacement and the pressure perturbation are neglected. As the pressure starts to decrease in the interaction region, it causes the flow in the viscous sublayer to "decelerate" (Figure 4 b). This is revealed by the observed "increase" of the displacement function (Figure 4 c, d).

An additional case tested the effect of the imperfections [circle Figures 5, Double circle (hump-dip) Figures 6] at the leading aircraft wing on the boundary layer. The pressure gradient and the displacement gradient are plotted, the pressure gradient is adverse as the flow approaches the circle and then becomes favorable until the crest of the circle. It then becomes less favorable in the recovery region of the flow.

Figure 5: Comparison of the four predictions for circle case

(a) Axial velocity; (b) radial velocity; (c) pressure gradient; (d) displacement gradient.

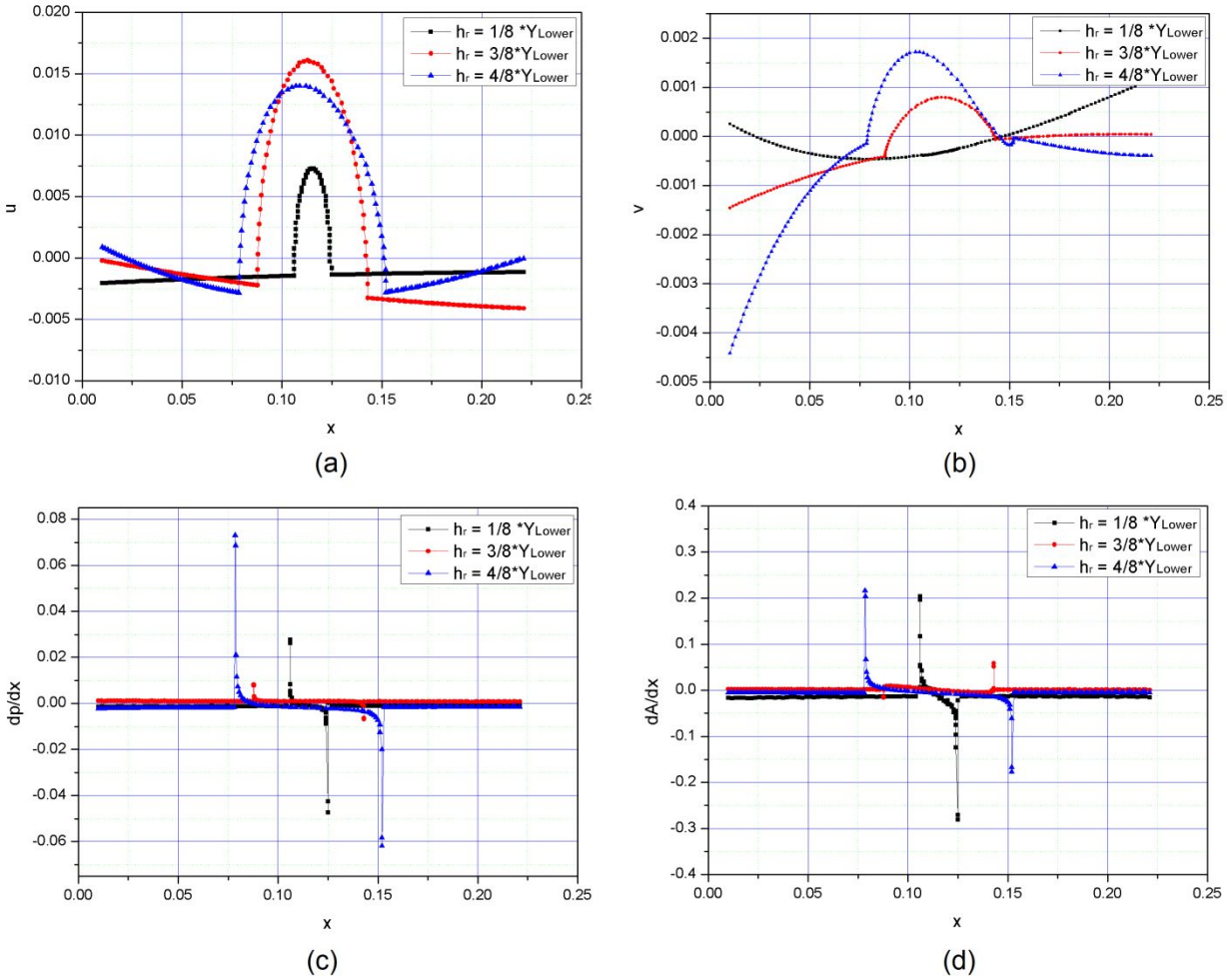

Figure 6: Double circele (hump-dip) case

(a) Contours; (b) pressure gradient; (c) displacement gradient.

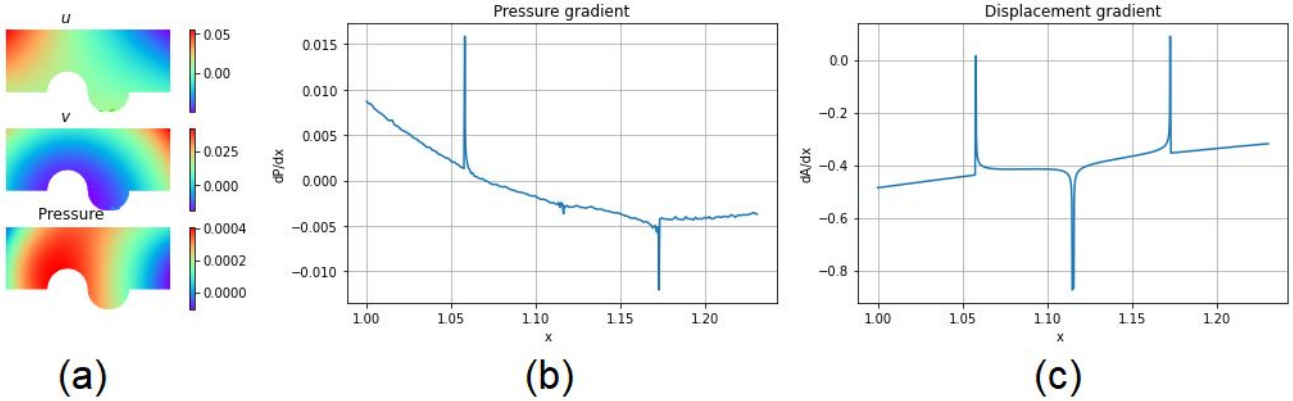

Figure 7 and Table 1 shows the computational domain and the grid structure for the hump adopted to RANS simulation (k–ω SST turbulence model). The flow is from left to right-hand side.

Figure 7: View of the Meshing Domain

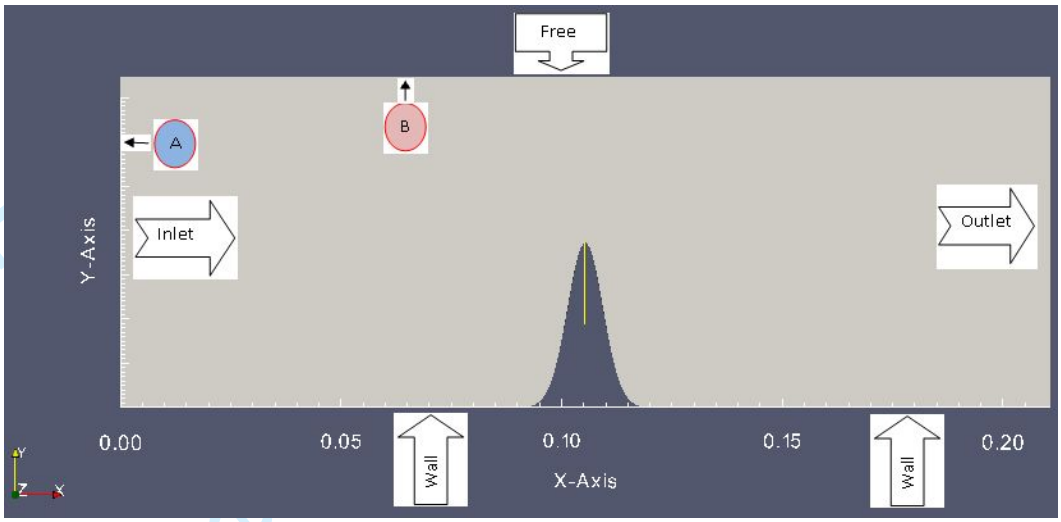

Table 1. Meshing Parameters

Edges	A	B	
Nodes	100	300	
grid size	30000		
Mesher Type	quadrilateral mesh		
y-plus	$y^+ = \frac{\sqrt{\frac{\tau_\omega}{\rho}}y}{\nu}$	y^+_{max}	O.118
		y^+_{mean}	0.025
Courant-Friedrichs-Lewy (CFL)	$C = \frac{u_x \Delta t}{\Delta x} + \frac{u_y \Delta t}{\Delta y}$	C_{max}	2.1162
		C_{mean}	5.9410^{-3}

The results presented here were normalized on the following conditions: Air at $20\,°C$ and 1 bar; Dynamic viscosity $\mu = 1.82 \times 10^{-5}\ N\,s\,m^{-2}$, Density $\rho = 1.19\,kg\,m^{-3}$. The boundary conditions are defined in Table 2.

Table 2: Boundary conditions of the

Boundary	Type	Value
Inlet	Free-stream	timeVaryingUniformFixedValue
Outlet	Pressure Outlet	zeroGradien
Bottom	Wall	No – Slip smooth
Top	Free- stream	zeroGradient

Furthermore, time dependency is a crucial factor of this study due to the unsteadiness of the flow field consisting of random and periodic pressure fluctuation occurring within the hump. Each time step was set as 0.25×10^{-5} seconds with an initial time equal to zero.

Figure 8 shows the density of mesh resolution near the walls and in the hump region

Figure 8 Mesh density hump case

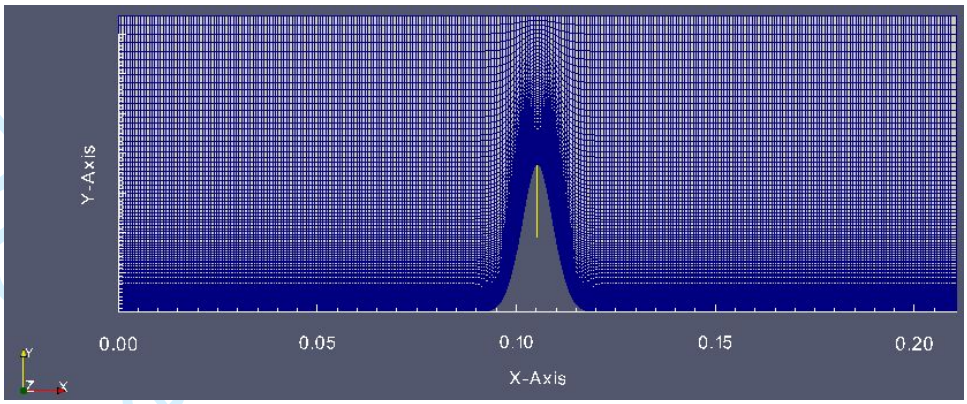

From Figure 9 it is possible to see an overall good agreement between triple-deck PINN's simulation and PisoFoam solvers with $k-\omega$ SST turbulence model.

Figure 9 Comparison of axial pressure gradient dp/dx, PINN and RANS approach for $\mathrm{h_r} = \frac{4}{8}\mathrm{Y_{Lower}}$

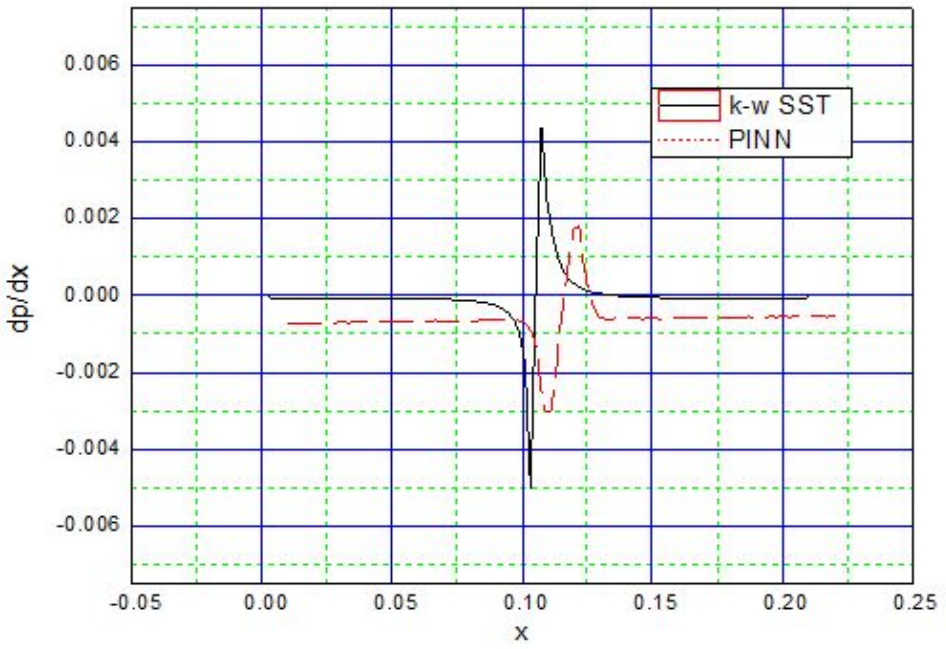

From the above figure, we can see how the difference between $k-\omega$ SST and Triple-Deck PINN's data in terms of dp/dx, in proximity to the hump, a larger acceleration of the flow in the $k-\omega$ SST results when compared to the Triple-Deck PINN's data. Also, the deceleration of the flow behind the hump is larger in the $k-\omega$ SST data when compared to the triple-deck PINN. We observe a zero pressure gradient along the wall axial direction in the $k-\omega$ SST when compared to the triple-deck PINN's data.

3.2 FLAT PLATE WITH LOCAL SURFACE HEATING

We present results of the Triple-Deck problem where subsonic flow past a local heating element that is placed on a flat surface (Figure 10).

Figure 10: Two-dimensional flow of a boundary layer over a flat heating element

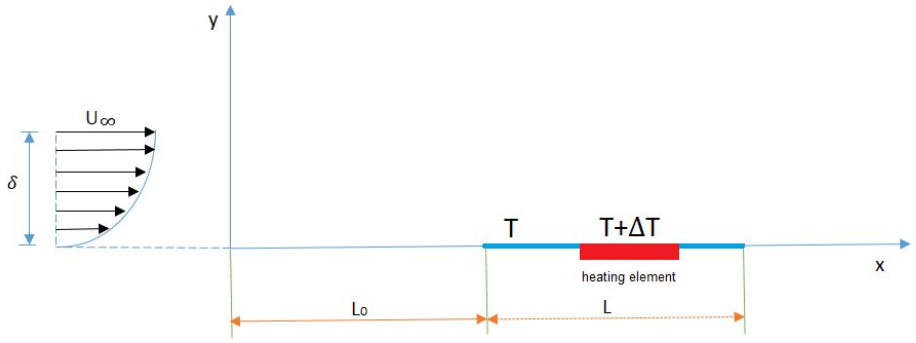

The size of the heating element r is $\frac{1}{4}Y_{Lower}$ while the wall temperature is given by

$$T(x) = \begin{cases} 1 + \Delta T & |x| \leq \frac{r}{2} \\ 1 & |x| > \frac{r}{2} \end{cases} \tag{18}$$

where ΔT is the amplitude of perturbations of the temperature Figure 11(a).

Figure 11: Temperature distributions for various values of ΔT

(a), the contour of velocity, pressure, and temperature (b)

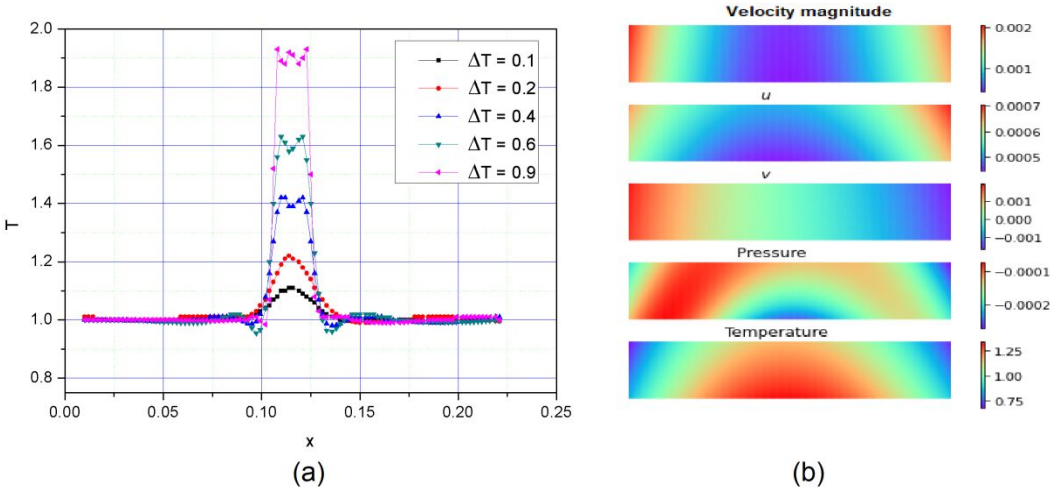

(a) (b)

In Figure 12 distributions of the axial velocity, pressure gradient, and displacement gradient are presented while ΔT varies. It can be observed that increasing the ΔT increases the pressure gradient and decreases the axial velocity and the displacement gradient which are located on the upstream

edge of the heating region and decreases the pressure gradient increases the displacement gradient which is located on the downstream edge of the heating region.

Figure 12: (a) Axial velocity, (b) pressure gradient, (c) Displacement and (d) displacement gradient distributions for various values of ΔT

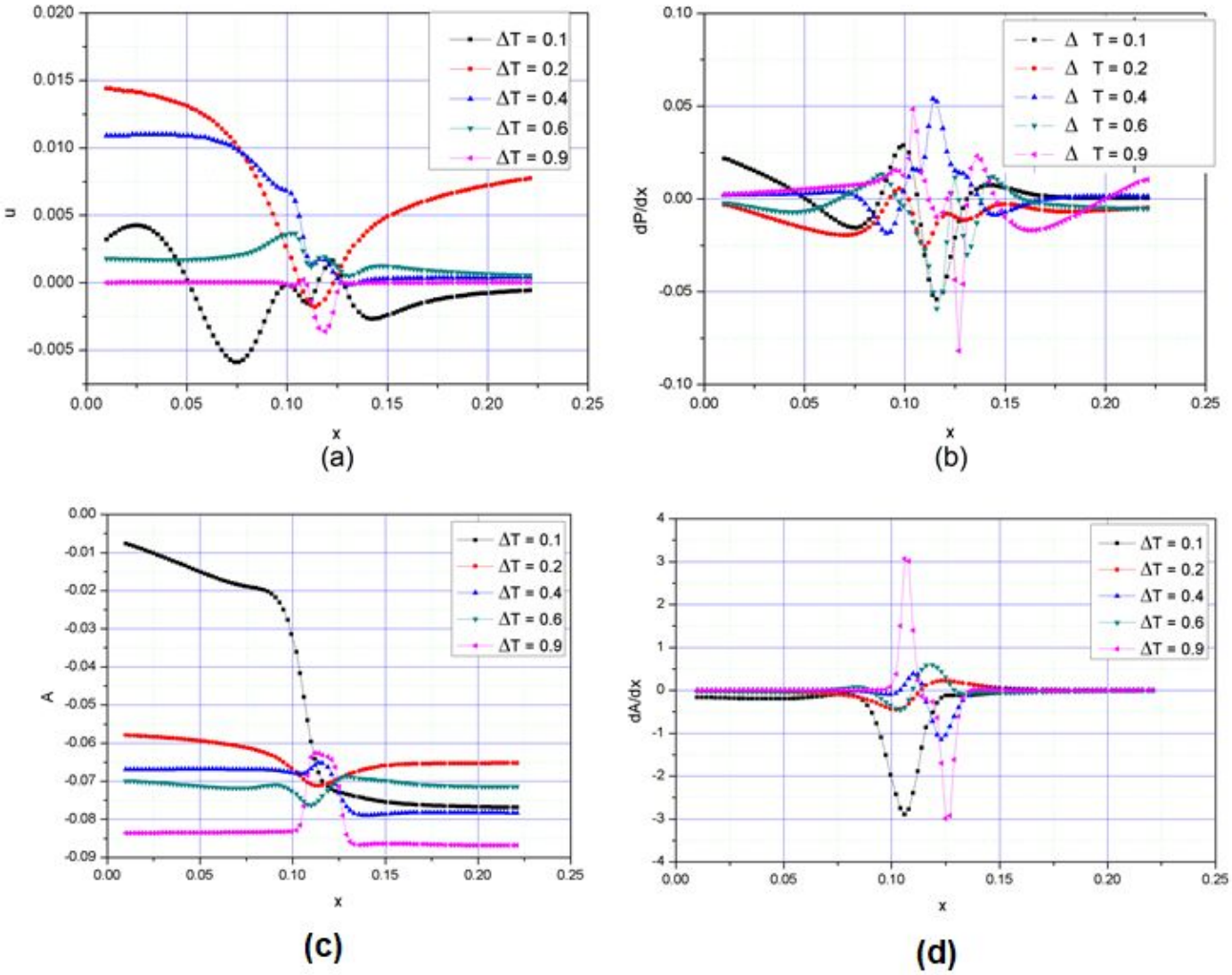

The displacement thickness of the boundary layer changes due to the effect of the surface temperature change that, in turn, induces a pressure perturbation in the external subsonic flow. The induced pressure perturbation exerts an effect on the region of slow boundary flow in which the main contribution to the change in the displacement thickness is formed. It has been shown that this situation leads to the formation of a local effective roughness on the surface and the problem

becomes similar to the problems considered above of the flow of a viscous gas over small irregularities Figure 11(b).

4 Conclusion

In this work, we have applied physics-informed neural networks (PINN) to two-dimensional steady-state laminar Navier-Stokes equations over a flat plate with a wavy surface of arbitrary amplitude and shape and specified local heating. We employ the Triple-Deck structure to describe the boundary-layer flow, which shows how a wavy surface and a local surface heating generates an interaction between the inviscid region and the viscous region near the flat plate. The Reynolds numbers were chosen to be relevant for aeronautical applications, while the shape and the related parameters can be seen as simple models of small deformation placed at the leading edge of the aircraft landing gear cavity. Clearly, the size, shape, and temperature of the surface elements are important factors to be taken into consideration in designing suitable forms which can be used to control the flow and separation of the boundary layer. Although for this particular application it is understood that effects of turbulence, unsteadiness of the flow may also be important, and should be included when considering the full problem.

Acknowledgments

The Computations were performed on the Al-Farabi Cluster computer of the Ecole Nationale Polytechnique Oran -MAURICE AUDIN.

References

Cousteix, J., & Mauss, J. (2007). “Asymptotic Analysis and Boundary Layers”, Springer.

Diesperov, V. N., & Korolev, G. L. (2003). “Formation of supersonic zones and local separation zones in transonic steady-state flow past surface roughness in the free interaction regime”. Fluid dynamics, 38(1), 43-50.

DU, Ke-Lin & SWAMY, M. N. S. (2014) “Fundamentals of machine learning. In : *Neural Networks and Statistical Learning”.* Springer, London. p. 15-65.

Gadd, G. E. (1957). “A theoretical investigation of laminar separation in supersonic flow”. Journal of the Aeronautical Sciences, 24(10), 759-771.

Hunt, J. C. R. (1971). “A theory for the laminar wake of a two-dimensional body in a boundary layer”. Journal of Fluid Mechanics, 49(1), 159-178.

Koroteev, M. V., & Lipatov, I. I. (2008). “Stationary subsonic boundary layer in the regions of local heating of surface”. arXiv preprint arXiv:0812.2513.

Koroteev, M. V., & Lipatov, I. I. (2009). “Supersonic boundary layer in regions with small temperature perturbations on the wall”. SIAM Journal on Applied Mathematics, 70(4), 1139-1156.

Koroteev, M. V., & Lipatov, I. I. (2012). “Local temperature perturbations of the boundary layer in the regime of free viscous–inviscid interaction”. Journal of fluid mechanics, 707, 595-605.

Koroteyev, M. V., & Lipatov, I. I. (2013). “Steady subsonic boundary layer in domains of local surface heating”. Journal of Applied Mathematics and Mechanics, 77(5), 486-493.

Lighthill, M. J. (1952). “On sound generated aerodynamically I. General theory”. Proceedings of the Royal Society of London. Series A. Mathematical and Physical Sciences, 211(1107), 564-587.

Lipatov, I. I. (2006). “Disturbed boundary layer flow with local time-dependent surface heating”. Fluid Dynamics, 41(5), 725-735.

Mengaldo, G., Kravtsova, M., Ruban, A. I., & Sherwin, S. J. (2015). “Triple-deck and direct numerical simulation analyses of high-speed subsonic flows past a roughness element”. Journal of Fluid Mechanics, 774, 311-323.

Messiter, A. F. (1970). “Boundary-layer flow near the trailing edge of a flat plate”. SIAM Journal on Applied Mathematics, 18(1), 241-257.

Neiland, V. Ya. (1969). “Theory of laminar boundary layer separation in supersonic flow”. Izv. Akad. Nauk SSSR, Mech. Zhidk. Gaza (4), 53-57

Raissi, M., Perdikaris, P., & Karniadakis, G. E. (2017). “Physics informed deep learning (part i): Data-driven solutions of nonlinear partial differential equations”. arXiv preprint arXiv:1711.10561.

Raissi, M., Perdikaris, P., & Karniadakis, G. E. (2019). “Physics-informed neural networks: A deep learning framework for solving forward and inverse problems involving nonlinear partial differential equations”. Journal of Computational Physics, 378, 686-707.

Schneider, W. (1974). “Upstream propagation of unsteady disturbances in supersonic boundary layers”. Journal of Fluid Mechanics, 63(3), 465-485.

Smith, F. T. (1973). “Laminar flow over a small hump on a flat plate”. Journal of Fluid Mechanics, 57(4), 803-824.

Smith, F. T., Brighton, P. W. M., Jackson, P. S., & Hunt, J. C. R. (1981). “On boundary-layer flow past two-dimensional obstacles”.Journal of Fluid Mechanics, 113, 123-152.

Stewartson, K. (1969). “On the flow near the trailing edge of a flat plate II”. Mathematika, 16(1), 106-121.

Stewartson, K., & Williams, P. (1969). “Self-induced separation”. Proc. Roy. Soc. A., 312.

Zeytounian, R. K. (2003). “Theory and applications of viscous fluid flows”. Springer Science & Business Media.

Symbols

δ - Boundary layer thickness

f - Surface waviness

A - Displacement function

ε – Perturbation paramter

R_e - Reynolds number

λ - Local scaled skin friction

Acronyms and Abbreviations

TdT - Triple-Deck Theory

PINN - Physics-Informed Neural Network

MSE - Mean Square Error

PDE - partial differential equations

RANS - Reynolds-averaged Navier–Stokes

.